



ELSEVIER

doi:10.1016/j.ultrasmedbio.2003.10.005

● *Original Contribution*

## THREE-DIMENSIONAL REGISTRATION OF PROSTATE IMAGES FROM HISTOLOGY AND ULTRASOUND

LAWRENCE S. TAYLOR,\* BRIAN C. PORTER,† GYONGYI NADASDY,‡  
P. ANTHONY DI SANT'AGNESE,§ DAVID PASTERNAK,† ZHE WU,† RAYMOND B. BAGGS,§||  
DEBORAH J. RUBENS<sup>¶</sup> and KEVIN J. PARKER<sup>†</sup>

Departments of \*Biomedical Engineering and †Electrical and Computer Engineering, University of Rochester, Rochester, NY, USA; ‡Department of Pathology, Ohio State University Medical Center, Columbus, OH, USA; Departments of §Pathology and Laboratory Medicine and ¶Department of Radiology, University of Rochester, Strong Memorial Hospital, Rochester, NY, USA; and ||Division of Laboratory Animal Medicine and of Environmental Medicine, University of Rochester Medical Center, Rochester, NY, USA

(Received 7 April 2003; revised 15 September 2003; in final form 2 October 2003)

**Abstract**—A whole mount histology protocol for 3-D tissue reconstruction to compare the size and spatial location of tumors (and other components) identified in histology data with that from 3-D ultrasound (US) images is presented. Prostate specimens are imaged in 3-D using B-mode (US) and sonoelastography. The prostate surface is outlined in each B-mode image and a 3-D surface reconstruction is made. The specimen is then prepared for whole mount histology and the histology slides are digitally reconstructed to make a 3-D surface. These two surfaces are then aligned using a 3-D correlation algorithm, and the tumor boundary determined by the pathologist is compared with that using sonoelastography. 3-D images showing the overlapping histology and sonoelastography of prostate surface reconstructions for one prostate are presented to illustrate the technique; results for four prostates yielded an accuracy of  $92\% \pm 3\%$ . (E-mail: [lstaylor@bme.rochester.edu](mailto:lstaylor@bme.rochester.edu)) © 2004 World Federation for Ultrasound in Medicine & Biology.

**Key Words:** Image registration, Three-dimensional ultrasound, Sonoelastography, Prostate cancer, Whole-mount histology, Fiducial markers.

### INTRODUCTION

Conventional diagnostic imaging techniques have been moderately useful for the *in vivo* detection of cancer in soft tissue, but a variety of advanced techniques are under investigation to increase the sensitivity and specificity of prostate tumor detection. We are developing a three-dimensional (3-D) ultrasound (US) imaging system called “sonoelastography imaging” to identify hard or stiff lesions within softer normal parenchyma and have imaged a series of excised (*in vitro*) whole prostates to control the many imaging parameters with greater accuracy than is possible *in vivo*. A whole mount pathology/histology protocol for 3-D tissue reconstruction has been developed to compare the geometry, size and spatial location of the tumor (or other lesions) from the 3-D

elasticity images with information from the “gold standard” histology data.

The pathologist traditionally looks at slides that effectively are 2-D images of a 3-D object. Multiple sections are taken at different planes to properly understand a 3-D organ. The advent of widely available 3-D image processing provides the pathologist with the additional tool of being able to segment structures of interest within an organ, then to view them within the organ as a whole. In this vein, Fix et al. (2000) overcame the problem of identifying the overall location and extent of lesions in a rat brain normally encountered using routine 2-D histopathologic evaluation. Lesions were induced by percutaneous injection of a toxin and then the organ was fixed and excised 3 days later, embedded in gelatin, frozen, then sectioned at 40- $\mu\text{m}$  intervals. A digital camera was used to acquire images of the sections and a 3-D reconstruction was performed using the IRIS Explorer (Numerical Algorithms Group, Downers Grove, IL) software. The 3-D reconstruction allowed for easy identifi-

Address correspondence to Lawrence S. Taylor, Hopeman Engineering Building, Room 310, Box 270168, University of Rochester, Rochester, NY 14627, USA. E-mail: [lstaylor@bme.rochester.edu](mailto:lstaylor@bme.rochester.edu)

cation of the exact location of the necrotic tissue within the overall brain structure. Moskalik et al. (2001) at the University of Michigan have developed a technique for aligning prostate histology with US frequency shift and power mode Doppler images. The reconstructed H & E histology slides are assembled into a 3-D volume to serve as a "gold standard" for comparison with the US data. The US and histology were aligned by modeling the prostate and urethra as an ellipsoid and a line, respectively. The surface and the line were then used to register the data for each prostate.

In an analogous method, we have developed a technique to acquire pathology information from excised prostates and to compare and contrast them with the corresponding tissue characterization from US elasticity images of the same tissue. Our ultrasonic imaging is performed immediately after surgical excision of the diseased prostate. 3-D images are reconstructed by assembling a series of 2-D US B-mode images. The geometrical accuracy of the US in the image plane depends only on how the actual speed of sound in a particular prostate differs from 1540 m/s, the speed assumed in the US scanner used. However, perpendicular to the scan plane, the accuracy is consistently high because movement of the imaging transducer in this direction, to generate a spatial sequence of 2-D images, is controlled by a precision stepper motor. Similarly, histology slices are taken at regular intervals and the histology images are digitized. Tissue shrinkage from histological preparation affects the apparent size of tissue (Schned et al. 1996). To compensate, the prostate histology is reconstructed, then scaled so that the size and volume of the whole prostate agrees with that of the 3-D B-mode image. The US serves as the "gold standard" or ground truth for the true size of the gland. The pathology characterized in the elasticity images is also reconstructed in 3-D and then compared with the resized histology after the two 3-D objects have been registered (Porter et al. 2001), making the resized histology the "gold standard" against which the elasticity imaging is judged.

#### *Background on sonoelastography*

The elasticity imaging technique used, sonoelastography, uses forced vibration as a means of distinguishing between hard cancerous lesions and softer healthy tissue. Vibration sonoelastography (or "sonoelasticity") imaging was first proposed for detection of hard tumors in the late 1980s (Parker et al. 1989). In this technique, low frequency ( $< 1000$  Hz) shear waves are propagated into deep tissue from an external vibration source, and real-time Doppler techniques are used to image the resulting vibration pattern on a US scanner. The low-frequency vibration is provided by an external source that is brought into contact with the patient or tissue sample. A

US transducer is then positioned to image the area of interest. When the propagating vibration enters the hard (elevated shear modulus) tumor, the amplitude of vibration decreases. Sonoelastography images this local decrease in vibration amplitude by mapping it to a grey scale or a color map. The underlying relative elasticity is then inferred from the resulting image. The amplitude of vibration within tissues is estimated and displayed using US pulse echo techniques specially designed for the Doppler signal of vibrating targets (Huang et al. 1990).

An analytic theory of tumor detectability in sonoelastography was developed by Gao et al. (1995). They proved that a small hard discontinuity in an otherwise uniform medium creates a disturbance in the vibration field that would otherwise not be present. Later, Parker et al. (1998) developed a finite element model for tumor detectability and showed the functional dependence of tumor contrast on frequency, tumor/background relative elasticity and lesion size.

We have previously demonstrated the detectability of phantom tumors of various sizes in phantom materials using this technique (Taylor et al. 1999), and have recently published a paper covering the principles and practices of 3-D sonoelastography (Taylor et al. 2000). Readers interested in additional details on imaging are directed to those sources. An example of sonoelastography tumor imaging is given in Figs. 3–6.

## MATERIALS AND METHODS

### *Ultrasound image acquisition*

This section describes the acquisition of B-mode and sonoelastography images of fresh prostate specimens. All patients in the study were diagnosed with prostate cancer and scheduled for a radical prostatectomy. Specimens were obtained from the operating room immediately after surgical excision and transported to the US area in the hospital. In preparation for imaging, the specimens were embedded in an agar gel (3–4% by weight in  $H_2O$ ) then placed on two thin parallel bars. The distance between the center lines of the bars was either 5 or 7.5 cm, which were found to provide the most uniform vibration in the tissue. The twin bar assembly was, in turn, mounted on a 100 lb-force (445 N) piston shaker (VTS, Aurora, OH) that provided the low-frequency vibration field required for the vibration imaging. The shaker was driven by an amplifier with voltage output that could be precisely controlled by a frequency generator. Low-frequency acoustical vibrations were then transferred to the agar-embedded specimen by means of the double bar arrangement.

After the sample had been placed in position, a 7-MHz linear-array transducer probe (a 739L from GE Medical) was secured above the middle of the tumor and

the vibration source was turned on. 3-D sonoelastography images of prostate were obtained by mounting the US transducer on a single-axis motorized track (Velmex, Bloomfield, NY) that was attached to a 3-D positioner. The motorized track was designed with a control box interface that allowed selection of the speed, direction and distance of motion. Movable limit switches were attached so that the track could be set to a predefined range of motion. The volume of interest was scanned by translating the transducer at a constant velocity normal to the image plane. The track speed was synchronized to the screen frame display rate to ensure that the transducer would move 1 mm in the sweep direction between the acquisition of color flow cine-loop frames. After image capture, the files were transferred from the scanner hard drive to an image-processing laboratory *via* a network connection.

#### *Preparation of gross specimens*

The radical prostatectomy specimen was received in saline after sonoelastography images had been obtained. The fresh prostate gland was weighed and measured. The measurements included apex to base, transverse and anterior-posterior maximum dimensions using calipers, and gland volume by means of fluid displacement. Two graduated cylinders were used to measure the fluid displacement. One was 1000 mL in size with 10 mL measuring lines and the other 100 mL marked with 1 mL lines. The larger cylinder allowed immersion of the whole gland. The smaller cylinder allowed measurement to the nearest marked line, introducing a round-off error of 0.5 mL. The resection margins of the gland were inked, with different colors representing each quadrant using the CDI tissue marking dye system (Cancer Diagnostic Inc., Birmingham, MI). A landmark device was obtained from Dr. Lars Egevad of Sweden (Egevad *et al.* 1998). The device, shown in Fig. 1, consists of two sets of four 3-mm diameter mating metal prongs, with each set attached to a metal base in a square grid pattern measuring either 13 × 13 mm or 19 × 19 mm, depending on the size of the specimen. The prongs were inserted in the specimen through the apex and the base symmetrically around the distal and proximal urethra, running parallel to the rectal surface of the prostate. The specimen then was fixed in 4% formalin for 48 h.

After fixation, the prongs were removed, leaving orientation holes for the matching of gross and microscope cross-sections and the gland was measured again, as above, to assess shrinkage. The prostate gland was then sectioned into 4 mm slices from the apex to the base using a commercially available food slicer (Krupps). Care was taken to ensure that the slices were cut parallel to each other. Depending on the size of the individual prostate, 6 to 10 gross pathology slices 3 to 5 mm thick

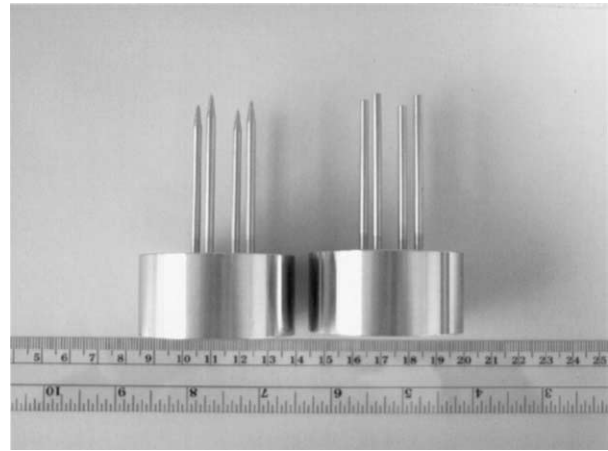


Fig. 1. Landmark device for creating internal fiducial markers in the prostate specimen. The four mating metal prongs form a square grid pattern that is used to align the sliced specimen into a 3-D volume after processing. The prongs are inserted in the specimen through the apex and the base parallel to the rectal surface of the prostate.

were produced. The end margin, or gland surface, proximal to the urinary bladder at the base was not included in the histological reconstruction. The amount of tissue removed varied from gland to gland, but always amounted to less than 1% of the gland volume. A slice thickness of 3 to 5 mm was used because it was found that thinner cuts resulted in slices of uneven thickness, which were very difficult to mount in cassettes. Thicker slices made surface reconstruction less accurate. The slices were then placed in a petri dish and marked to orient each individual piece. The specimen was then transferred to the imaging facility (see later) for photographic imaging.

#### *Preparation of cassettes*

Upon receipt back from the imaging facility, tissues from the petri dishes were transferred to super cassettes (Surgipath Medical Industries, Richmond, IL). The cassettes were placed on a VIP tissue processor (Sakura, Torrance, CA) with an 11-h processing schedule consisting of various grades of ethyl alcohol, xylene and Paraplast™. The processed whole-section prostate slices were embedded in Paraplast™, using large metal base molds (Surgipath Medical). Sections 4–5 μm thick were cut from the surface of each block and placed on glass slides. The slides were baked for 1 h at 60°C and stained using routine hematoxylin-eosin protocol. The result was one histology slide for each gross slab.

The microscope whole-mount sections (histology slides) were examined by two pathologists (G. Nadasdy and P. A. di Sant'Agnes) "blinded" to the sonoelastography results. The areas of carcinoma and benign nodular

hyperplasia were outlined with two different color marking pens and the slides were then sent for computer imaging and comparison with the sonoelastography results.

#### *Imaging of pathology/histology data*

Both the gross pathology slices and the histology cassettes were photographed after preparation, so that 3-D reconstruction could be performed. Color image capture of both the gross prostate slices and the histology slides was accomplished using digital photography (Diagnostic Spot RT color digital camera, Diagnostic Instruments Inc, Sterling Heights, MI). The petri dish or slide was placed on a flat table, above which the camera was mounted in an assembly so that the focal plane was parallel to the table top. After they were acquired, images were transferred to a Dell Dimension XPS H266 computer and archived using the Advanced Spot camera software (Diagnostic Instruments). For the gross specimens, a caliper was used to measure the thickness of each slice to provide the third dimension for our 3-D reconstruction. After the images were captured, Adobe Photoshop version 5.5 was used to align each slice so that 3-D reconstruction could be achieved by reconstructing the images as a stack. This was accomplished by visually aligning the fiducial marker holes, made by the landmark device described earlier, in each image successively. The images were then passed on to the image-processing laboratory for 3-D reconstruction.

#### *Reconstruction of histology and ultrasound data*

For each prostate, 3-D volumes were created from 2-D ultrasound B-mode images and images of histology slides. The US data are regarded as the "gold standard" or ground truth because they are acquired before tissue fixation and cassette preparation. A 3-D image of the prostate surface is produced from the US data in the following manner. The US volume is reconstructed by extracting a set of 2-D B-mode images from cine sequence, acquired at 1-mm intervals. The images are manually segmented to designate prostate tissue from background agar under the supervision of the team radiologist. A binary mask of the prostate cross-section is produced and assembled into a 3-D volume that is validated by comparison with the fluid displacement specimen volume and the fresh caliper measurements from pathology. The sequence of 2-D images is then read into IRIS Explorer to create a 3-D surface volume with 1-mm voxels. The corresponding B-mode volume is stored at the original resolution.

3-D representations of prostate boundaries and tumor volumes are produced from histology slide images. The dimensions of the 2-D histology images are corrected for shrinkage by first comparing the histology slides with the gross slab photographs, then comparing

the caliper measurement with the US surface reconstruction. Figure 2 shows an example of the tissue distortion sometimes observed when comparing an original slab with the resulting slide. The prostate gland is segmented from background and an edge detector is applied to the segmented images to create outlines of the gland. Automatic edge detection was used because the grey-level transition at the gland boundary is high and the regions inside and outside are sufficiently homogeneous to allow a local derivative operation. At this point, it should be recalled, the histology volume is sparsely sampled (one image per 3–5 mm) in the z-axis dimension (apex-base), because only one histology slide is made from the surface of each cassette-embedded gross pathology slice. To create a smooth prostate surface, the captured slides are interpolated in the x–y plane at 1-mm spacing, using the method of shape-based interpolation of multidimensional objects (Raya and Udupa 1990). First, a "distance field" image is generated from each edge-detected histology gland boundary. The distance field image is created so that each pixel value in the image is equal to the closest distance from this pixel location to the gland boundary, with a plus or minus sign indicating whether this pixel is in or out of the boundary. Then, the series of "distance field" images are interpolated at 1-mm intervals, using spline interpolation. Finally, a contour line is drawn at zero pixel value level on each interpolated field image. These contour lines are the interpolated gland boundaries. The same procedures apply to the tumor traced by the pathologist and other components of interest within the volume. The final surface volume is reconstructed in IRIS Explorer with 1-mm voxels. The corresponding histology image volume is stored as 0.25 mm × 0.25 mm × 1 mm voxels, with the tumor volume stored as 1-mm voxels.

#### *Registration of histology and ultrasound data*

The US and histology surface volumes are registered using a semiautomatic correlation search algorithm to find the best match for surface voxel overlap. This method has been described in previous work (Porter et al. 2001). The two surface volumes are input to the program that runs in the IRIS Explorer environment on an Indigo2 workstation. After a user manually orients the prostate surfaces, the algorithm searches through a defined range in six degrees of freedom, three translation and three rotation. As the surface voxels approach alignment, the correlation value increases. For two identical registered volumes, the correlation value should be 1. The correlation calculation is given by:

$$\frac{|R_{fg}(T)|^2}{R_{ff}R_{gg}} \leq 1 \quad (1)$$



Fig. 2. Distortion effects from processing the gross slab into a slide. The left image shows a gross section of the prostate after fixing and cutting. Note the four holes from the landmark device described in Fig. 1. The right image shows the resulting slide after the slab has been processed. The anterior-posterior axis (vertical) has been scaled more than the transverse axis (horizontal). The blue dots indicate the tumor region on the slide.

where  $R_{fg}(T)$  is the correlation of overlapping volumes for a given position.  $T$  refers to a transformation consisting in general of three translations and three rotations. In terms of continuous mathematics,  $R_{fg}(T)$  is defined as:

$$R_{fg}(T) = \int_{-\infty}^{\infty} \int_{-\infty}^{\infty} \int_{-\infty}^{\infty} f^*(x,y,z)g^T(x,y,z)dx dy dz \quad (2)$$

where  $f(x,y,z)$  is the prostate surface from histology in the Cartesian coordinate system  $(x,y,z)$ ,  $f^*(x,y,z)$  is the complex conjugate of  $f(x,y,z)$ ,  $g(x,y,z)$  is the prostate surface from ultrasound and  $g^T(x,y,z)$  is the US prostate surface after the six degrees of freedom rigid transformation.  $R_{ff}$  and  $R_{gg}$  are included in eqn (1) to normalize the equation. They are the autocorrelations for the individual surface representations and are calculated by the integral:

$$R_{ff} = \int_{-\infty}^{\infty} \int_{-\infty}^{\infty} \int_{-\infty}^{\infty} f^*(x,y,z)f(x,y,z)dx dy dz \quad (3)$$

The best matching orientation is used to remap the US data into the histology frame of reference. The final registered volume shows corresponding sonoelastography-delineated tumors and tumors outlined by pathology for position comparison.

## RESULTS

In this section, a case study showing all phases of US gland surface reconstruction and registration with the reconstructed prostate histology is presented. After registration of the surfaces has been achieved, it is used to align and compare the histology and sonoelastography 3-D tumor renderings. Following this, results from four

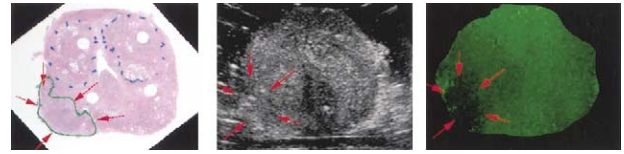


Fig. 3. 2-D prostate images of the same region of an excised prostate specimen (case 12). The histology image on the left has been prepared using an H & E stain. The pathologist has outlined the cancerous region in green, as indicated by the red arrows. BPH is outlined with blue dots. The center image is the B-mode US image of the same plane. Note that the cancer is not visible. The image on the right is the sonoelastography image. In this image, vibration amplitude has been mapped to a color scale; bright green = high vibration, dark green = low vibration. The cancer is visible as a region of low vibration marked by red arrows.

cases demonstrating the accuracy and repeatability of the registration process, are presented.

### Example number 1

Figure 3, from case study number 12, illustrates the basic concept of sonoelastography tumor imaging. It shows transverse histology, B-mode US and sonoelastography images of an excised prostate. The B-mode and sonoelastography images were acquired simultaneously by the scanner and are coregistered.

In the sonoelastography image (right), vibration amplitude has been mapped to a green scale, where high vibration is bright green and low vibration is dark green. A vibration signal of three pure tones (80, 133, 187 Hz) was used during image acquisition. Because the tumor is stiffer (elevated elastic modulus) than the surrounding tissue, it vibrates with a lower amplitude. The area of reduced vibration has been marked by red arrows that can be seen in the left posterior prostate. The red arrows in the B-mode (middle) image mark the same location where the tumor is visible in the sonoelastography image. The tumor is isoechoic in the B-mode image.

The histology image (left) in Fig. 3 is of a slice nearby to that imaged by the US. The familiar H & E stain coloration is visible, along with four circular holes that were produced by the landmark device. Also visible, at the center of the slide, is the verumontanum. Benign prostatic hyperplasia (BPH) has been outlined with blue dots and the cancerous tissue has been outlined in green, illustrating that the cancerous tissue correlates well with the area and location of the vibration deficit in the sonoelastography image.

Figure 4 shows the 3-D reconstruction of the prostate surface using histology, shown in purple on the left, and US, shown in green on the right. Reconstruction was performed as described earlier. These two data sets were used to do the registration illustrated in Fig. 5, where

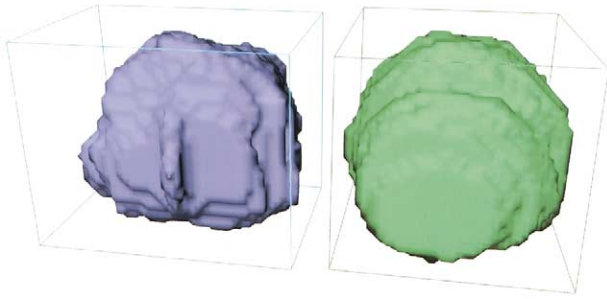


Fig. 4. 3-D reconstruction of the prostate surface. The histology is shown in purple on the left and US is shown in green on the right.

purple and green are, respectively, the histological and US prostate surfaces. We used the intersection of both data sets divided by the B-mode volume as a metric for the accuracy of how well the volumes align. The image registration experiment shown in Fig. 5 yielded a value of 94%.

Figure 6 shows the results of the registration of the sonoelastography tumor (yellow) with the histology tumor reconstruction (red). The two viewpoints are of the same object taken from different positions to better illustrate how the objects correlate. The sonoelastography (yellow) has been rendered as transparent to help show the interpenetration of the two objects. The view on the

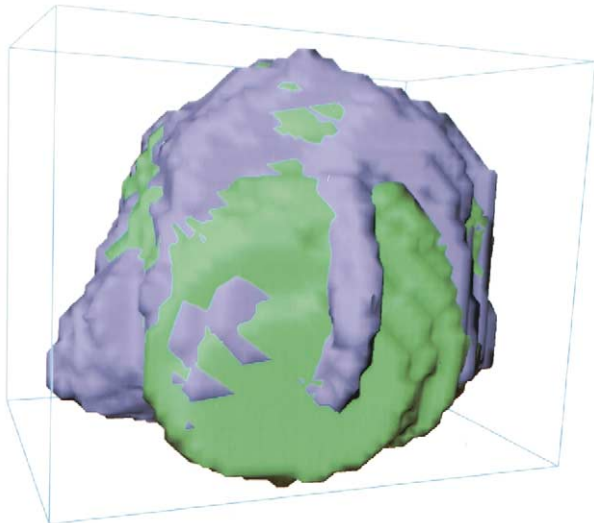


Fig. 5. 3-D surface fusion of case 12. The histology (purple) and US (green) gland surfaces shown in Fig. 4 have been registered using a semiautomatic correlation search algorithm that maximizes the correlation between the surface voxels. The best match is shown. This alignment has been used to compare the location of the histology with sonoelastography tumors in Fig. 6.

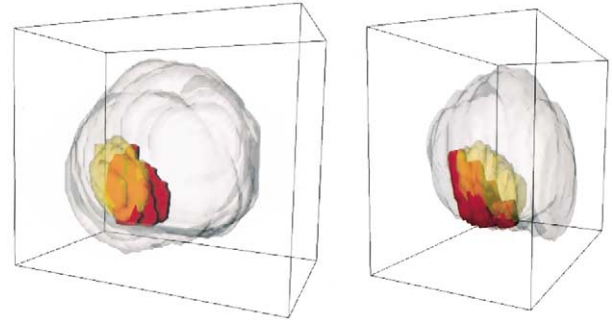


Fig. 6. Tumor registration of case 12 using the surface registration shown in Fig. 5. Two viewpoints are shown. The B-mode gland surface is shown in a transparent grey. The histology tumor is red and the one from sonoelastography is yellow. In the image on the right, the histology tumor (red) is seen to protrude outside the gland surface, indicating that there is distortion in histology surface reconstruction.

left side of Fig. 6 is almost a base side axial view, with the left side of the gland on the left side of the image and the right side on the right. It shows that the sonoelastography 3-D tumor reconstruction (yellow) is located slightly (about 4 mm) toward the base relative to the histology. The volume of the histology tumor is measured to be 1216 mm<sup>3</sup>, and the sonoelastography tumor measured at 1490 mm<sup>3</sup>. However, the volume of the overlap of the two objects was 477 mm<sup>3</sup>, suggesting an imperfect surface registration. In the broader study, there were eight cases where the tumor volume exceeded 1.0 mL. In this group, the average tumor size as measured by pathology was  $3.1 \pm 2.1$  mL and the average tumor size as measured by sonoelastography was  $2.8 \pm 1.6$  mL.

#### Data from four cases

In this section, results from four cases are presented to illustrate the repeatability and the accuracy achieved in this method. The B-mode 3-D reconstruction of the gland is validated by comparison with the fluid displacement volume of the gland. This tests the accuracy of the manual segmentation of the prostate surface. The 3-D histology volume is reconstructed after scaling factors are applied to obtain the histology volume as close as possible to the B-mode volume. This histology gland surface is registered with the surface generated from the B-mode sequence. After surface registration, the enclosed volumes are analyzed and the overlapping volume or intersection is divided by the B-mode volume as a metric for registration accuracy. If the reconstruction and registration are perfect, that value will be one.

Table 1 summarizes the accuracy data for four cases. The column header *Fluid vol* in Table 1 refers to

Table 1. Registration accuracy for four cases

Case	Fluid vol (mL)	B-mode vol (mL)	Hist vol (mL)	Accuracy (%)
31	30	29	31	89
33	36	32	35	94
39	27	23	22	90
42	38	36	36	94

The fluid volume in column 1 is used to validate the accuracy of the US volume shown in column 2. Column 3 is the rescaled histology gland volume.

the volume of the gland after the seminal vesicles have been removed, but before the tissue has been fixed or processed. The accuracy of the fluid displacement measurements is rated at  $\pm 1/2$  mL, based on the round off error associated with using a graduated cylinder with marked lines of 1 mL. A good B-mode segmentation, “*B-mode vol*”, should match this volume quite closely. The column title “*Hist vol*” gives the value of the histology gland volume after the anisotropic scaling. “*Accuracy*” refers to the intersection of the two registered volumes normalized by the B-mode volume.

## DISCUSSION

Several factors affect the accuracy of this method, with accuracy of the surface reconstruction being the key because it determines the ultimate quality of the registration. Segmenting the B-mode images is usually straightforward, although errors are possible. The excised glands are embedded in an agar gel to enable the applied vibration to penetrate the gland. This creates an echogenic region around the gland surface. This can be seen in Fig. 3 in the center image. To validate that an accurate B-mode segmentation has been made, the segmented gland volume from the B-mode is compared with the gland fluid displacement volume before fixation and histologic processing. In some cases, outlining of the gland in the B-mode images was validated with the histology.

Reconstructing the histology presents its own challenges. Because cutting the prostate into slices less than 3 to 5 mm thick was found to be impractical, histology must be sampled by digital photography at 3–5 mm intervals in the apex-base direction. This is due to the fact that each gross prostate slab makes one cassette and each cassette produces only one histology slide from its surface. Using these samples alone to reconstruct the gland surface results in a staircase-type effect. Because the US is sampled at 1 mm intervals, this makes the surface registration, which is the key process in aligning the two volumes, less accurate. To compensate for this low resolution in the apex-base axis, interpolation was

used to provide for a smoother surface. This, of course, assumes that the surface is sufficiently smooth so that the 3–5 mm sample rate gives a good reconstruction.

One source of error in this technique is the distortion to the surface caused by the four-prong device. The device is essential for the 3-D reconstruction of the histology volume, but it introduces a nonuniform change in the shape of the gland surface. To minimize these effects, the protocol for impaling was changed during the study. At the beginning of the study, the unfixed tissue was impaled, then sliced. Later, the tissue was fixed first, then impaled. The latter procedure resulted in less distortion of the final histology cross-sections.

Another source of error is the nonuniform distortion during the slide preparation procedure. A histology slide is produced by cutting a thin slice of tissue from a slab of prostate. After mounting on the microscope slide, the cross-sectional shape of the prostate on the slide does not necessarily match the original shape of the prostate slab from which it was cut. Each slide/slab pair from a particular prostate may have different shrinkage or expansion factors, due to forces acting on the thin specimen during mounting, so one scale factor cannot correct all the slides in one specimen. To create a prostate surface that better approximates the original shape, each histology slide is compared with its corresponding gross section and scaled if necessary.

Finally, it should be pointed out that, although our application is for a sonoelastography imaging system, any 3-D US technique could be used. This would include contrast-enhanced B-mode images, elastography strain images, color Doppler images and tissue characterization techniques. The only requirement is that the imaging modality must be coregistered with a sequence of B-mode images.

## SUMMARY AND CONCLUSIONS

We have presented a method of soft tissue image registration using the correlation of two surfaces. Ultrasound B-mode and histology images of the same gland were acquired and reconstructed into volumes. After surface registration, the histology tumor delineation and sonoelastography tumor were compared to verify the accuracy and validity of the imaging system. It has been shown that image registration, previously shown to be effective for vessel registration, is viable for whole-gland surface registration. We believe that this process should be a minimum standard for validating 3-D images in all cases, and for 2-D images when prior alignment of the image plane and histology plane cannot be guaranteed. Although our examples are from an elasticity imaging case, any 3-D US imaging system can be validated using this technique.

*Acknowledgments*—This work was supported in part by the NSF/NYS Center for Electronic Imaging Systems, the University of Rochester Departments of Radiology and Electrical Engineering, the General Electric Company (GE) and a grant from the NIH (2 RO1 AG16317-01A1). The authors thank Dr. Edward M. Messing, who provided the whole-gland specimens, sacrificing tissue harvested for his own research. The authors also thank GE Medical Systems Division for the loan of the Logiq 700 US scanner used in the imaging experiments.

## REFERENCES

- Egevad L, Engstrom K, Busch C. A new method for handling radical prostatectomies enabling fresh tissue harvesting, whole mount sections, and landmarks for alignment of sections. *J Urol Pathol* 1998;9:17–28.
- Fix A, Stitzel S, Ridder G, Switzer R. MK-801 neurotoxicity in cupric silver-stained sections: Lesion reconstruction by 3-dimensional computer image analysis. *Toxicol Pathol* 2000;28:84–90.
- Gao L, Alam S, Lerner R, Parker K. Sonoelasticity imaging: Theory and experimental verification. *J Acoust Soc Am* 1995;97:3875–3886.
- Huang S, Lerner R, Parker K. On estimating the amplitude of harmonic vibrations from the Doppler spectrum of reflected signals. *J Acoust Soc Am* 1990;88:310–317.
- Moskalik A, Rubin M, Wojno K, et al. Analysis of three-dimensional Doppler ultrasonographic quantitative measures for the discrimination of prostate cancer. *J Ultrasound Med* 2001;20:713–722.
- Parker K, Fu D, Gracewski S, Yeung F, Levinson S. Vibration sonoelastography and the detectability of lesions. *Ultrasound Med Biol* 1998;24:1437–1447.
- Parker K, Huang S, Musulin R, Lerner R. Tissue response to mechanical vibrations for “sonoelasticity imaging.” *Ultrasound Med Biol* 1989;16:241–246.
- Porter B, Strang J, Rubens D, Parker K. Three-dimensional registration and fusion of ultrasound and MRI using major vessels as fiducial markers. *IEEE Trans Med Imag* 2001;20:354–359.
- Raya S, Udupa J. Shape-based interpolation of multidimensional objects. *IEEE Trans Med Imag* 1990;9:32–42.
- Schned A, Wheeler K, Hodorowski C, et al. Tissue-shrinkage correction factor in the calculation of prostate cancer volume. *Am J Surg Pathol* 1996;20:1501–1506.
- Taylor L, Porter B, Rubens D, Parker K. 3-D sonoelastography for prostate tumor imaging. In: *Proceedings of the International ICSC Congress on Computational Intelligence: Methods and Applications ICSC*: Academic Press, 1999:468–472.
- Taylor L, Porter B, Rubens D, Parker K. Three-dimensional sonoelastography: Principles and practices. *Phys Med Biol* 2000;45:1477–1494.